Nanoscale Res Lett (2009) 4:618–626
DOI 10.1007/s11671-009-9286-x

NANO EXPRESS

Biocompatible Nanocomplexes for Molecular Targeted MRI Contrast Agent

Zhijin Chen · Dexin Yu · Shaojie Wang · Na Zhang · Chunhong Ma · Zaijun Lu

Received: 16 December 2008 / Accepted: 5 March 2009 / Published online: 18 March 2009

Abstract Accurate diagnosis in early stage is vital for the treatment of Hepatocellular carcinoma. The aim of this study was to investigate the potential of poly lactic acid–polyethylene glycol/gadolinium–diethylenetriamine-pentaacetic acid (PLA–PEG/Gd–DTPA) nanocomplexes using as biocompatible molecular magnetic resonance imaging (MRI) contrast agent. The PLA–PEG/Gd–DTPA nanocomplexes were obtained using self-assembly nanotechnology by incubation of PLA–PEG nanoparticles and the commercial contrast agent, Gd–DTPA. The physicochemical properties of nanocomplexes were measured by atomic force microscopy and photon correlation spectroscopy. The T_1-weighted MR images of the nanocomplexes were obtained in a 3.0 T clinical MR imager. The stability study was carried out in human plasma and the distribution in vivo was investigated in rats. The mean size of the PLA–PEG/Gd–DTPA nanocomplexes was 187.9 ± 2.30 nm, and the polydispersity index was 0.108, and the zeta potential was -12.36 ± 3.58 mV. The results of MRI test confirmed that the PLA–PEG/Gd–DTPA nanocomplexes possessed the ability of MRI, and the direct correlation between the MRI imaging intensities and the nano-complex concentrations was observed ($r = 0.987$). The signal intensity was still stable within 2 h after incubation of the nanocomplexes in human plasma. The nanocomplexes gave much better image contrast effects and longer stagnation time than that of commercial contrast agent in rat liver. A dose of 0.04 mmol of gadolinium per kilogram of body weight was sufficient to increase the MRI imaging intensities in rat livers by five-fold compared with the commercial Gd–DTPA. PLA–PEG/Gd–DTPA nanocomplexes could be prepared easily with small particle sizes. The nanocomplexes had high plasma stability, better image contrast effect, and liver targeting property. These results indicated that the PLA–PEG/Gd–DTPA nanocomplexes might be potential as molecular targeted imaging contrast agent.

Keywords Nanocomplexes · Molecular imaging · Magnetic resonance imaging · DTPA–Gd · PLA–PEG

Introduction

Hepatocellular carcinoma (HCC) is one of the most dreaded diseases in the world, which brings dramatic increases in morbidity and mortality both in the developed and developing countries. Accurate diagnosis in early stage is vital for the treatment of patients. Presently, routine screening strategies such as ultrasound every 6 months have been recommended for early detection in patients with liver cirrhosis to detect HCC at earlier stage. Magnetic resonance imaging (MRI) is one of the most useful technologies in the field of diagnostic imaging [1]. However, the sensitivity and specificity of conventional MRI are far from satisfactory. The development of molecular imaging provide an unprecedented opportunity for the diagnostic detection rate of HCC.

Z. Chen · N. Zhang (✉)
School of Pharmaceutical Science, Shandong University, 44 Wenhua Xi Road, 250012 Ji'nan, People's Republic of China
e-mail: zhangnancy9@sdu.edu.cn

D. Yu · C. Ma
Department of Radiology Medicine, Affiliated Qilu Hospital, Shandong University, 44 Wenhua Xi Road, 250012 Ji'nan, People's Republic of China

S. Wang · Z. Lu (✉)
School of Chemistry and Chemical Engineering, Shandong University, 27 Shanda Road, 250012 Ji'nan, People's Republic of China
e-mail: z.lu@sdu.edu.cn

The key elements of molecular MRI are: (1) increasing the sensitivity and specificity of the visualization procedure; (2) improving the selectivity in tissue characterization; (3) reducing the intrinsic image artifacts; and (4) acquiring more functional information on the imaged processes [2]. Therefore, the preparation of the special imaging probes with high specificity is the key elements.

Gadolinium–diethylenetriamine pentaacetic acid (Gd–DTPA, commercial product named as Magnevist®) is the most commonly used MRI contrast agent that shortens the T_1 longitudinal relaxation time of protons of water and increases the contrast of the image because the contrast agent shortened relaxation time. However, there are significant problems such as short half-life in blood and lack of specificity to target organs and tissues for diagnosis of this low molecular weight contrast agent. Furthermore, when Gd–DTPA was injected intravenously, they were located in extracellular fluid and rapidly cleared from the body. Therefore, Gd–DTPA was not suit for molecular MRI. In order to resolve this problem, many nano-carrier systems have been examined for the increases in relaxivity and specificity. The carriers including proteins [3], dendrimers [4, 5], linear polymers [6, 7], and micelles [8] have been proposed and evaluated as molecular MRI contrast agents. DTPA or another chelating unit was conjugated to these carriers. None of these, however, has achieved the increase both in relaxivity and in specificity. Therefore, studies on molecular contrast agents special for liver with relatively longer metabolic time and stable contrast effect in liver tissue are still highly desired.

At present, polymer micelles combined with gadolinium are very promising because of their ability to provide positive contrast (i.e., T_1-weighted images), robust structural features, and simple fabrication. In such a micelle assembly product, the rate of water exchange is similar to that observed in Gd–DTPA, because the Gd complex is exposed in the exterior shell layer of the micelle [9]. The micelle that made of macrocyclic 1,4,7,10-tetraazacyclododecane-1,4,7,10-tetraacetic acid (DOTA) has been studied by Andre et al.[9]. However, the DOTA was not biocompatible. Therefore, it is necessary to study some biocompatible contrast agent. Poly lactic acid–polyethylene glycol (PLA–PEG) is one of the commonly used diblock copolymer with hydrophilic and hydrophobic blocks. It allows the formation of a stable nano-particulate suspension in an aqueous solvent, where PLA chains form the core and PEG chains are located outside [10]. The PEG shell prevents the interaction of PLA core with biomolecules, cells, tissues, and can suppress opsonization [11]. The PLA–PEG micelle had been successfully used for drug delivery by Pierri [12], but the micelle was not suitable for the molecular contrast agent because the micelles mostly stay within lymph fluid rather than accumulation in the nodal macrophages and rapidly move via the lymphatic pathway [13]. Furthermore, the micelle structure may dissociate in the bloodstream into a single polymer chain, and the gadolinium will be rapidly excreted out of the body, which was not advantage to diagnose [14]. Reportedly, PLA–PEG nanoparticles show a particle size of several dozen to a few hundred nanometers, and possess a hydrophilic and inactive surface of PEG, leading to a longer systemic circulation [15]. Therefore, the main purpose of this study is to investigate the possibility of the core–shell PLA–PEG nanoparticles to be used as novel target molecular MRI contrast agent nano-carriers for the diagnostic detection of HCC.

First, the core–shell PLA–PEG nanoparticles were prepared, and then the Gd–DTPA was absorbed to the surface of the PLA–PEG nanoparticles by self-assembly nanotechnology to obtain the nanocomplexes as contrast agent for molecular MRI. The formulation was tested for physical parameters such as particle size, zeta potential, image contrast effect, and the stability in human plasma. The gadolinium content of the nanocomplexes was determined by inductively coupled plasma-atomic emission spectroscopy. The distribution in vivo was studied in rats after intravenous injection to confirm the targeting property.

Materials and Methods

Materials

Wistar rat were purchased from the experimental animal center of Shandong University. All animal test procedures were performed in accordance with the National Institutes of Health guidelines on the use of animals in research. MRI was conducted under anesthesia by intraperitoneal injection of pentobarbital (50 mg/kg of body weight).

PLA–PEG ($MW_{PLA} = 48{,}000$ Da, $MW_{PEG} = 4{,}000$ Da) was a gift kindly provided by School of Chemistry and Chemical Engineering of Shandong University (Jinan, China). Gadopentetic acid dimeglumine salt injection (Gd–DTPA, Magnevist®) was purchased from Bayer Schering Pharma AG. All other chemicals were of analytical reagent or higher grade.

Preparation of the Nanocomplexes

Preparation of PLA–PEG Blank Nanoparticles

The PLA–PEG blank nanoparticles were produced by modified solvent diffusion method [16]. Briefly, 1.5 mL organic polymer solution (40 mg of PLA–PEG dissolved in methylene chloride) was dropped into 25 mL EtOH at 8 mL/h (KdScientific U.S.A) under moderate stirring, leading to the immediate polymer precipitation. Subsequently, in

order to facilitate the collection of the particles, 25 mL of Milli-Q water was added to the nanoparticles suspension, and the stirring was maintained for 10 min. Finally, the organic solvents were eliminated by evaporation under vacuum at 37 °C and the blank nanoparticles were collected.

Preparation of PLA–PEG/Gd–DTPA Nanocomplexes

The nanocomplexes were produced by self-assemble nanotechnology. Briefly, 1.0 mL of Gd–DTPA solution (0.5 mmol/mL) was added dropwise to 7 mL of PLA–PEG blank nanoparticles suspension under gentle vortexing for 20 s. Subsequently, the sample was incubated at room temperature for 30 min to facilitate complexation. The nanocomplexes were obtained by centrifuging at 15,000 rpm for 30 min at 4 °C (Shanghai Anting Scientific Instrument Co., Ltd, China), washed thrice by Milli-Q water, subsequently resuspended in Milli-Q water, and filtered through a membrane with 0.80 μm pore size (Phenomenex, 25 mm filter, CA, USA). The gadolinium content of the nanocomplexes was determined by inductively coupled plasma-atomic emission spectroscopy.

Investigation the Physico-Chemical Properties of the Nanoparticles and the Nanocomplexes

Transmission Electron Microscopy (TEM) and Photon Correlation Spectroscopy (PCS) Analysis

The size and morphology of nanoparticles were examined using a transmission electron microscope (JEM-1200EX, Jeol, Japan). A carbon-coated 200-mesh copper specimen grid was glow-discharged for 1.5 min. One drop of nanoparticle suspension was deposited on the grid and allowed to stand for 1.5 min after which any excess fluid was removed with filter paper. The grid was later stained with one drop of 2% aqueous solution of sodium phosphotungstate for contrast enhancement. The grids were allowed to dry for an additional 10 min before examination under the electron microscope.

Size and zeta potential of the nanocomplexes were analyzed in triplicates by photon correlation spectroscopy and laser Doppler anemometry, respectively, using a particle sizer (Zetasizer 3000 HAS, Malvern Instruments Ltd., Malvern, Worcestershire, UK). Samples were analyzed after appropriate dilution in MilliQ water. Reported values were expressed as mean ± standard deviation for at least three different batches of each nanocomplexes formulation.

Atomic Force Microscopy Imaging (AFM)

Atomic force microscopy observation was performed in air at room temperature, on a Dimension 3000 apparatus, as well as on Multimode Equipment, both monitored by a Nanoscope IIIa controller from Digital Instruments (Santa Barbara, CA, USA). A droplet (5 μL) of sample was deposited on a freshly cleaved silicon surface, spread and partially dried with a stream of argon. The images were obtained in tapping mode (Tapping mode atomic force microscopy, TM-AFM), using commercial silicon probes, from Nanosensors^{TM}, with cantilevers having a length of 228 μm, resonance frequencies of 75–98 kHz, spring constants of 29–61 N/m, and a nominal tip curvature radius of 5–10 nm. The scan rate was 1 Hz. Dimensional analyses were performed using the "section of analyses" program of the system. A minimum of 10 images from each sample was analyzed to assure reproducible results.

Magnetic Resonance Imaging In Vitro

In vitro MRI test was performed with a 3.0 T magnet at Philips Achieva 3.0T MRI (Philips Co., Netherlands). The T_1-weighted MR images of the prepared nanocomplexes and a commercially available contrast agent, Gd-DTPA, were obtained. MR images were taken with different concentrations of Gd solution (1×10^{-4} to 1×10^{-3} mM Gd/L). The blank PLA–PEG nanoparticles were taken as the control. The experimental condition was as follows: TR (repetition time) = 5.2 ms, TE (echo delay time) = 2.1 ms, flip angle: 4.0, field of view: 26×20 cm^2.

Stability of the Nanocomplexes in Human Plasma

The stability of the nanocomplexes was determined in the presence of 50% human plasma at 37 °C. Two-hundred microliters of nanocomplexes were incubated with 200 μL of human plasma at 37 °C for 0, 0.5, 1.0, and 2.0 h, respectively. To isolate nanocomplexes from human plasma, the mixture was separated by centrifugation at 15,000 rpm for 30 min at 4 °C, washed thrice, and subsequently resuspended in Milli-Q water. The each resuspension was determined by MRI. The particle size was determined by TEM after incubation in plasma and compared with the freshly prepared sample.

Evaluation of In Vivo Distribution

Twelve Wistar rats were examined to evaluate the in vivo distribution of the nanocomplexes. Animals were divided into two groups, receiving either Gd–DTPA ($n = 6$) or PLA–PEG/Gd–DTPA nanocomplexes ($n = 6$). The rats were imaged on a 3-Tesla clinical scanner (Philips Co., Netherlands) using a knee coil array comprised two modified Alderman-Grant resonators. A tail vein cannula consisting of a 30-gauge needle attached to Tygon tubing (2.0 m length) was then established. The two image agents were injected via the tail vein catheter with an infusion

pump (6 mL/min). A 0.04 mmol/kg body weight aliquot of the contrast agent solution was injected. The targeting efficiency (TE^C) of nanocomplexes were calculated and compared with Gd–DTPA to evaluate the tissue targeting property after intravenous administration. Targeting efficiency (TE^C) was calculated from Eq. 1. The mean area under the curve (AUC) of PLA–PEG nanocomplexes concentrations in organs was calculated by the trapezoidal method during the experimental period ($AUC_{[0-8]}$)

$$TE^C = \frac{AUC_{nanocomplexes}}{AUC_{Gd-DTPA}}. \quad (1)$$

Results

Characterization of the Nanocomplexes

The morphology of PLA–PEG blank nanoparticles and the PLA–PEG/Gd–DTPA nanocomplexes was investigated using transmission electron microscopy. The nanoparticles and the nanocomplexes had spherical or ellipsoidal shapes (Fig. 1). Results of size and zeta potential measurements by PCS are shown in Table 1 and Fig. 2. The size of the nanopcomplexes was smaller than 200 nm. The result of AFM showed that the blank nanoparticles were 56 nm. The nanocomplexes were 70 nm, which was larger than the blank nanoparticles in dried state (Figs. 3, 4). The size of PLA–PEG and nanocomplexes was 56 and 70 nm, respectively, in the AFM image, which was different from that observed by PCS. It might be explained that the AFM image was taken at the drying condition and the PCS was taken at the suspension. The PEG chain of the nanocomplexes was extended in the suspension and folded at the drying state.

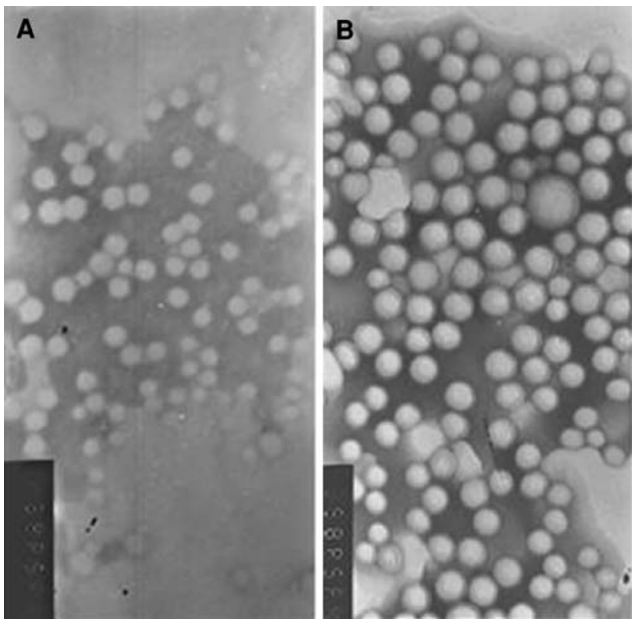

Fig. 1 TEM results of the blank nanoparticles and the nanocomplexes

Table 1 Result of physicochemical properties of the nanoparticles and the nanocomplexes

	Size (nm)	Polydispersity index	Zeta potential (mV)
Blank nanoparticles	146.87 ± 3.10	0.107	−15.72 ± 4.88
Nanocomplexes	187.9 ± 2.30	0.108	−12.36 ± 3.58

Magnetic Resonance Imaging

In order to assess the effect of increasing amounts of Gd–DTPA on the complexes image enhancement, the doses of Gd–DTPA from 1×10^{-4} to 1×10^{-3} mmol/mL were tested. The image intensity increases and the T_1 relaxation time shorten as a function of the amount of contrast agent included in the complexes (Fig. 5). The results of MRI test confirmed that the PLA–PEG/Gd–DTPA nanocomplexes possessed the ability of MRI, and the direct correlation between the MRI intensities and the nanocomplexes concentrations was observed ($r = 0.987$). The blank PLA–PEG nanoparticles did not enhance the signal intensity, which confirmed the Gd–DTPA was absorbed to the surface of the nanoparticles.

Stability of the Nanocomplexes in Human Plasma

The results of the stability experiment showed that the nanocomplexes' morphology did not change after incubation for 2 h as observed under TEM (data not shown). The MRI signal intensity of the nanocomplexes decreased after incubation with the plasma for 2 h, but no noticeable difference was detected ($P > 0.05$). The result of the experiment indicated that the nanocomplexes were stable in human plasma for at least 2 h (Fig. 6).

Magnetic Resonance Imaging In Vivo

Images of the in vivo experiment with Gd–DTPA in rat were displayed in Fig. 7. In the preinjection image, the vena cava, the kidneys, and the liver were dark owing to the choice of the inversion delay (Fig. 7a, e).

After injection of Gd–DTPA (30 s), the urinary bladder became extraordinary lighter (236.54 ± 24.72 to 960.6 ± 27.56) owing to the introduction of the contrast agent. The kidney was bright also and the signal intensity was increased from 278 ± 13.64 to 923 ± 19.02 (Fig. 7b),

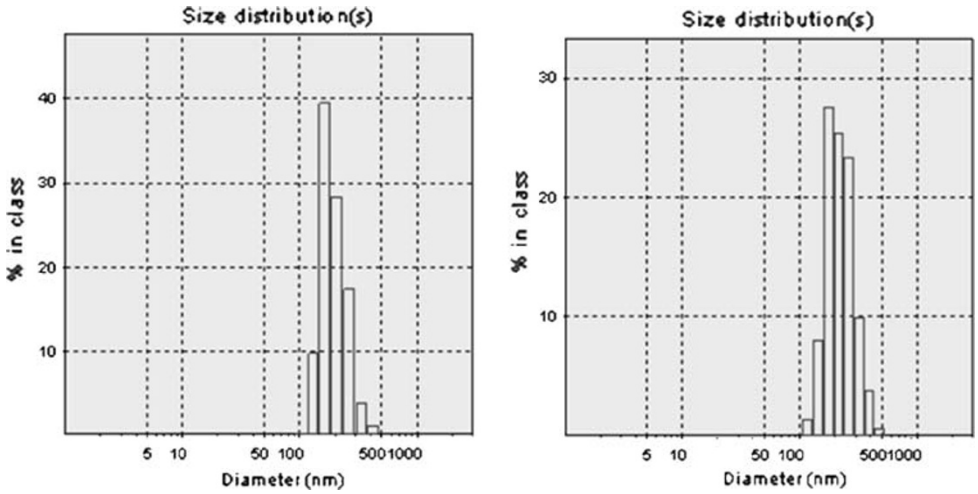

Fig. 2 Size distribution of the blank nanoparticles and the nanocomplexes

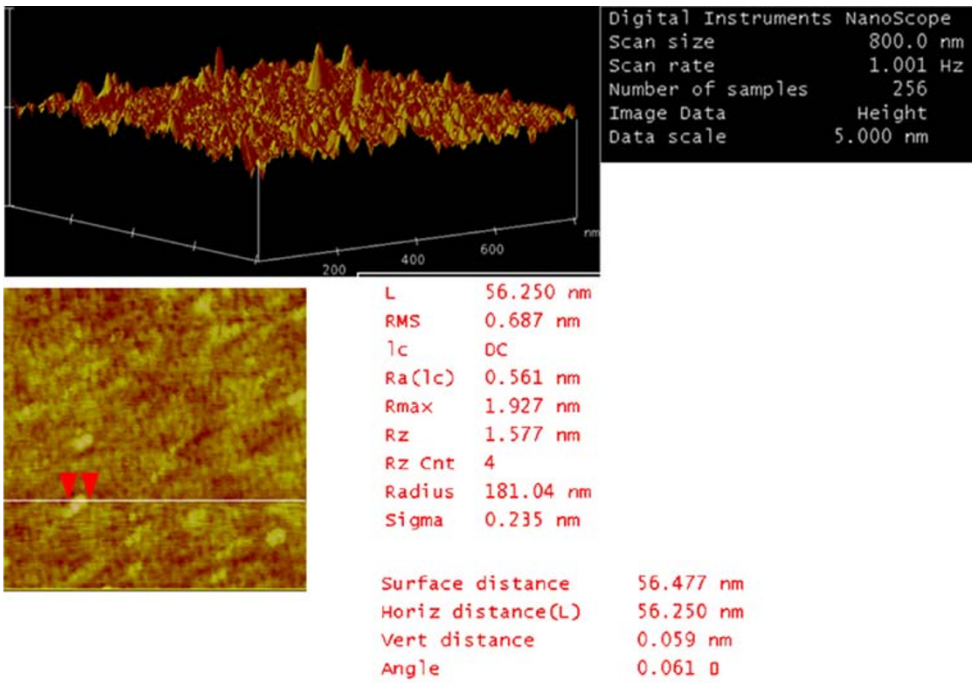

Fig. 3 AFM images of PLA–PEG blank nanoparticles showing spherical obtained in tapping mode. Scan sizes are 800 nm

followed by a rapid decay in signal intensity. As shown in Fig. 7c, the signal intensity of the liver had increased from 302 ± 16.67 to 504 ± 21.01 at 60 s after injection. The whole body of the rat was as dark as preinjection 1 h later following injection of Gd–DTPA (Fig. 7d).

The signal intensity in the liver gradually increased after injection of the nanocomplexes compared with the Gd–DTPA (shown Fig. 7f, g). One hour later, the signal intensity of the liver reached the highest (from 309 ± 14.21 to 482 ± 11.91), and then attenuated slowly (Fig. 7g). The enhanced signal intensities of the liver continue 4 h after injection of the nanocomplexes, while continued 10 min only after injection Gd–DTPA. The contrast intensity–time curves of the rat liver after injection of Gd–DTPA and PLA–PEG/Gd–DTPA nanocomplexes were shown in Fig. 8. The slow rising of intensity curve of nanocomplexes might be attributed to the gadolinium released slowly from the complexes. The AUC (area under contrast intensity–time curves) enhancement of the nanocomplexes was 4.98-fold greater than that of Gd–DTPA. The kidneys and urinary bladders became lighter gradually, and reached the highest within 2 h postinjection of the nanocomplexes (271 ± 25.32 to 703 ± 36.7 for kidneys and 279 ± 28.51 to 1578 ± 35.08 for urinary bladders). From the scheme, the enhancement was not significantly different in the lung between the two contrast agents at the same time in vivo.

The in vivo distribution result of the nanocomplexes was shown in Fig. 9. The results of the TE^C confirmed that the nanocomplexes were targeted to the muscle and the heart,

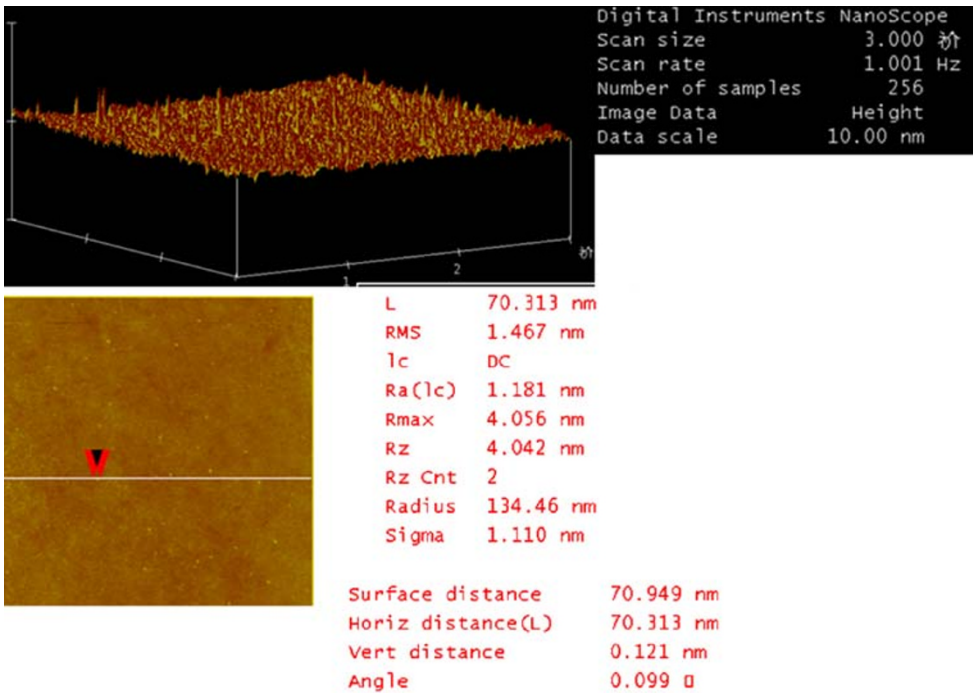

Fig. 4 AFM images of PLA–PEG/Gd–DTPA nanocomplexes showing spherical obtained in tapping mode. Scan sizes are 3 μm

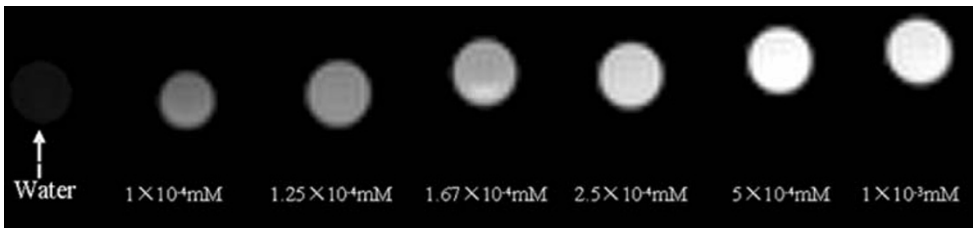

Fig. 5 Imaging intensity of nanocomplexes dependent on the dose of Gd–DTPA

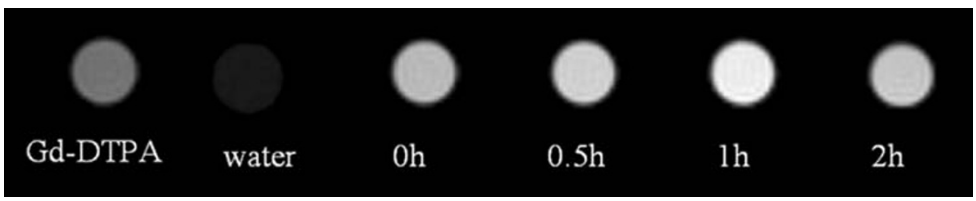

Fig. 6 Stability of the nanocomplexes in human plasma

which was not macroscopic. The TE^C of the liver was 4.98, which indicated that the nanocomplexes can effectively concentrate to the liver and enhance the signal intensity (Table 2).

Discussion

The blank PLA–PEG nanoparticles prepared by modified solvent diffusion method were homogeneous with respect to the minor polydispersity index (<0.2) and can be considered monodisperse. The nanocomplexes were smaller than 200 nm, which could be considered optimal for Stealth® systems to prevent the filtering in the spleen and increase the uptake by macrophages [17]. It is evident from the results of PCS experiments that the hydrodynamic diameter of the nanoparticles in the solvated state is larger than that obtained from TEM experiments [18]. Some authors have demonstrated that the mean diameter of nanoparticles has an influence on the biodistribution studies. The particles within the 150–200 nm range were found to be longest circulating [19, 20], and so the PLA–PEG/Gd–DTPA nanocomplexes, with sizes around 200 nm, could be particularly interesting to reach the loose junctions of the endothelium of cancer or infectious foci, considering the mean sizes measured by PCS. Nanoparticle with mean diameters of 190 nm was selected for use because the nanoparticle accessing to hepatocytes through the hepatic sinusoidal wall requires the passage through endothelial cell pores that are estimated at 150–200 nm [21]. Zeta potential results (Table 1) showed

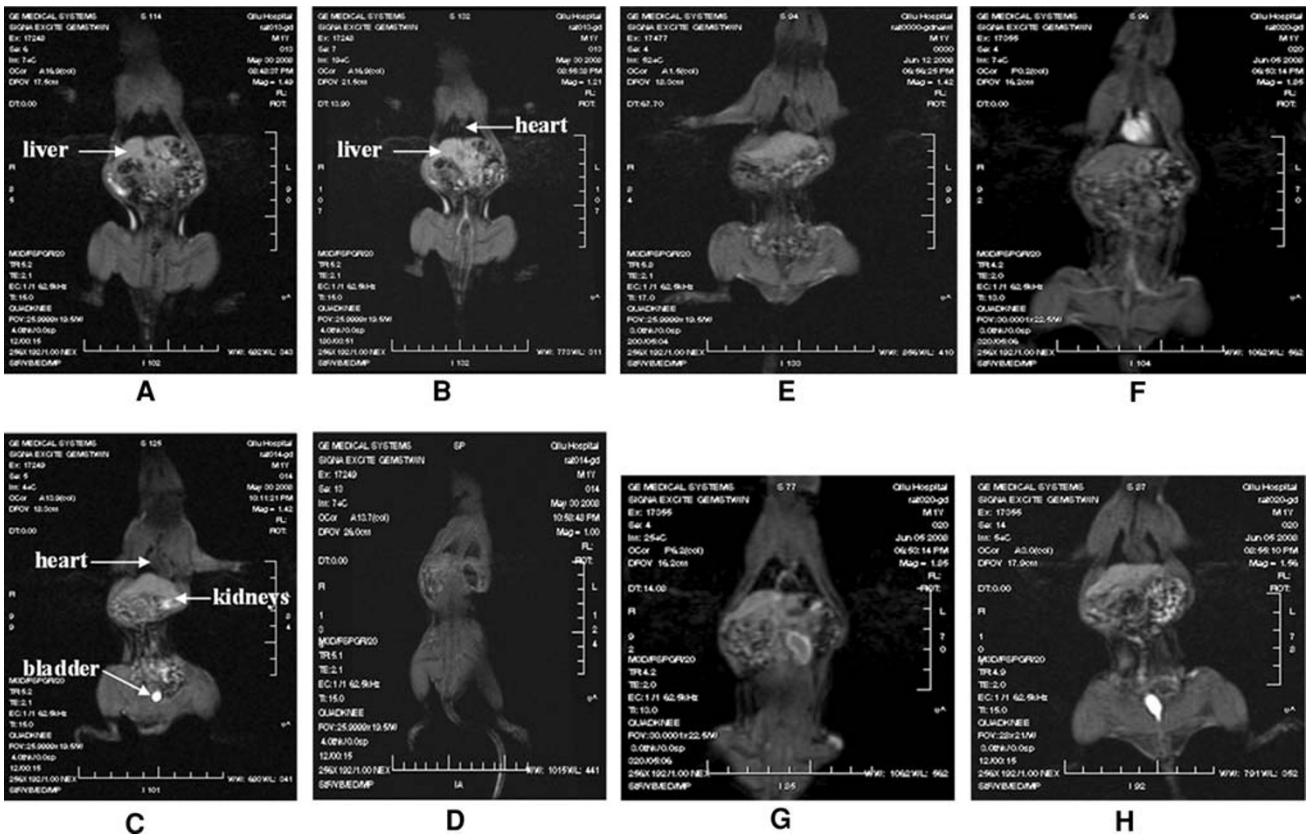

Fig. 7 Imaging of Gd–DTPA and PLA–PEG/Gd–DTPA nanocomplexes in vivo

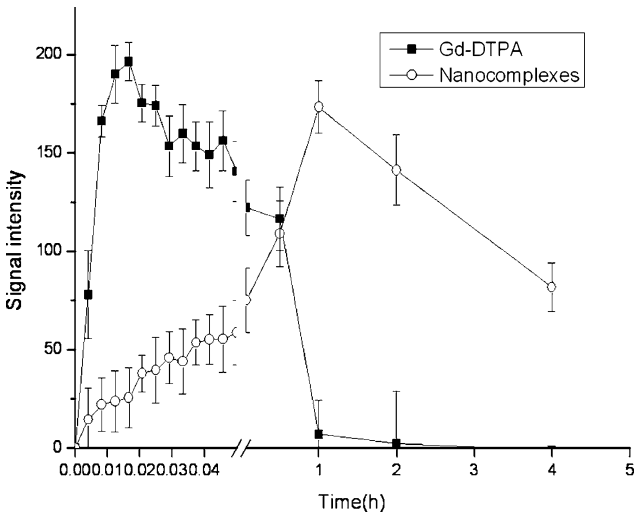

Fig. 8 The contrast enhanced intensity-time curves of rat liver after injection of Gd–DTPA and nanocomplexes

that the blank PLA–PEG nanoparticles and PLA–PEG/Gd–DTPA nanocomplexes exhibited a negative charge with values ranging from −12.36 to −15.72 mV. The nanoparticles have moderately anionic surface potentials (at the plane of hydrodynamic shear) to minimize nonspecific uptake. Cationic particles are internalized nonspecifically through proteoglycan receptors and may stick to anionic cell surface membranes, while highly anionic polystyrene nanoparticles have increased nonspecific uptake by scavenger receptors following complement activation [22, 23].

The Gd–DTPA loaded PLA–PEG nanoparticles belong to self-assembly nanotechnology. Therefore, the self-assembly nanotechnology between like-charge has been study for years [24, 25]. Messina et al. [26] have investigated the complexation of highly charged sphere with long flexible polyelectrolyte, both negatively charged in a salt-free environment. They observed multilayer of the highly charged polyelectrolyte chains confined to the sphere for lower charge density, the polyelectrolyte chain wrapped around the sphere. A mechanism involving Coulomb coupling was proposed to explain the structures. In our design, the PLA–PEG nanoparticle would be seen as the charged sphere and the Gd–DTPA was seen as the polyelectrolyte, and the nanocomplexes formulation could be explained by the Coulomb coupling theory. Piroll et al. [27] also have prepared liposome complexes with Gd–DTPA by the same mechanism.

Contrast of the nanocomplexes was substantially improved and remained unchanged for at least 2 h after incubation with the human plasma. This stability in human plasma was contributed to the PEG chain of the

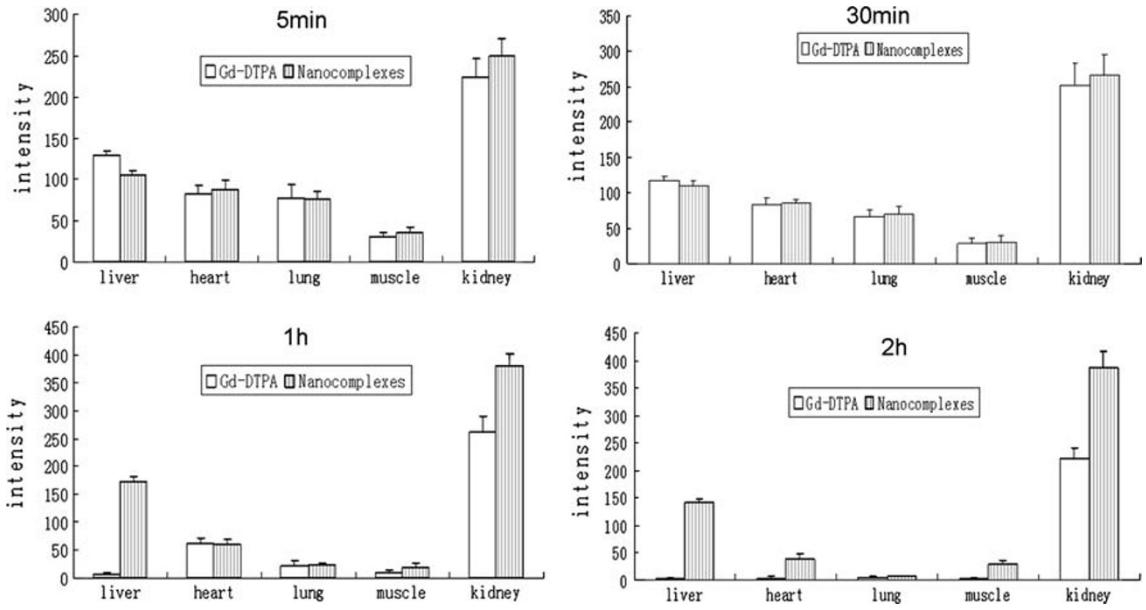

Fig. 9 Distribution in vivo of the Gd–DTPA and nanocomplexes in rats after intravenous injection

Table 2 Result of the AUC of the enhanced intensity of the Gd–DTPA and the nanocomplexes ($n = 6$)

	$AUC_{(0–8\ h)}$		TE^C
	Gd–DTPA	Nanocomplexes	
Liver	99.11 ± 14.68	493.78 ± 16.67	4.98
Lung	1.29 ± 0.35	1.13 ± 0.41	0.88
Heart	43.80 ± 8.56	84.46 ± 12.31	1.92
Muscle	13.21 ± 7.32	191.69 ± 15.60	14.51
Kidney	232.18 ± 29.32	1218.15 ± 67.69	16.95

nanocomplexes. Folding of the PEGs leads to the formation of PEG coils including Gd–DTPA molecules, which are compactly bound to the ether groups of the PEG chains, and the water molecules were loosely bound to the PEG chains [28]. Therefore, a heavily hydrated coating layer consisting of conformational random PEG chains covers the underlying surface [29, 30]. Therefore, the surface is protected against adsorbing proteins because of the unfavorable entropy change that results in compression of this coating layer [30]. In addition, the negative charges of the nanocomplexes could prevent the nanocomplexes from plasma protein binding. If serum proteins bind to the surface of nanocomplexess, the cross-linking between nanocomplexes would be expected to occur. However, this phenomenon was not observed from TEM after incubation.

The signal intensity of the nanocomplexes was dependent on the Gd–DTPA concentration, which was absorbed onto the surface of the nanocomplexes. The correlation coefficient of the signal intensity and the concentration of the Gd–DTPA nanocomplexes was 0.987. Thus, the concentration of the nanocomplexes could be determined by the signal intensity in vivo at different times. The results of the imaging experiment in vitro showed that the blank PLA–PEG nanoparticles did not enhance the signal intensity, which confirmed the Gd–DTPA was absorbed onto the surface of the nanoparticles.

A dose of 0.04 mmol of gadolinium per kilogram of body weight was sufficient to increase the liver signal by 4.98-fold after injection of the nanocomplexes compared with Gd-DTPA. Contrast was substantially improved and remained for 4 h after administration. In contrast, the Gd–DTPA solution just remained for 10 min.

Comparing the intensity results in Figs. 8 and 9, the highest signal intensity was not increased by the nanocomplex. In addition, the highest intensity in liver was similar with the Gd–DTPA injection. The nanocomplexes enhanced the retention time of Gd–DTPA in vivo and increased the live distribution due to the passive target mechanism. Furthermore, the contrast of the nanocomplexes lasted for 4 h that is longer than the free Gd–DTPA, which is the advantage of diagnosing in the clinical. The delayed signal of the nanocomplexes was benefit for diagnosing in the clinical. The signal intensity of free Gd–DTPA decreased too quickly to obtain accurate images and so it was difficult to observe the different organs or different parts of organs after a single injection. It is possible to observe and compare different organs or different parts of the organs carefully due to the enhanced retention time of the nanocomplexes. More accurate diagnosis and more precise conclusion would be obtained due to the delayed signal intensity. The kidneys were become brightly after 2 h administration of the nanocomplexes seems to be

related to the delayed blood clearance compared with Gd–DTPA. On the other hand, this result could suggest that the nanocomplexes have a renal elimination [31]. Of course, such a route of excretion can only be confirmed by urine measurement of the Gd concentration, but this nanocomplexes size that allow their retention in kidney are known to be freely excreted through the fenestrated capillaries of the kidney [32].

Conclusion

The PLA–PEG blank nanoparticles were prepared by modified solvent diffusion method. Then, the Gd–DTPA was absorbed onto the surface of the nanoparticles to obtain the nano complexes by self-assembly nanotechnology. The nanocomplexes were stable in human plasma at least for 2 h. The results of the biodistribution experiments confirmed that the nanocomplexes had long stagnation time in the liver and could target to the liver. In summary, we have successfully demonstrated the feasibility of the experimental biodegradable (Gd–DTPA) nanocomplex contrast agent to perform effective MRI in rats.

Acknowledgments The research was supported by the national science foundation for post-doctoral scientists of China (20070421081) and the specialized fund for the post-doctoral creative program of Shan dong province of China (200703065).

References

1. G. de Marco, A. Bogdanov, E. Marecos, A. Moore, M. Simonova, R. Weissleder, Radiology **208**(1), 65 (1998)
2. R. Weissleder, Radiology **212**(3), 609 (1999)
3. T.N. Nagaraja, K. Karki, J.R. Ewing, R.L. Croxen, R.A. Knight, Stroke **39**, 427 (2008). doi:10.1161/strokeaha.107.496059
4. H. Xu, C.A.S. Regino, Y. Koyama, Y. Hama, A.J. Gunn, M. Bernardo, H. Kobayashi, P.L. Choyke, M.W. Brechbiel, Bioconjug. Chem. **18**, 1474 (2007). doi:10.1021/bc0701085
5. H. Xu, C.A.S. Regino, M. Bernardo, Y. Koyama, H. Kobayashi, P.L. Choyke, M.W. Brechbiel, J. Med. Chem. **50**(14), 3185 (2007). doi:10.1021/jm061324m
6. X.X. Wen, E.F. Jackson, R.E. Price, E.E. Kim, Q.P. Wu, S. Wallace, C. Charnsangavej, J.G. Gelovani, C. Li, Bioconjug. Chem. **15**(6), 1408 (2004). doi:10.1021/Bc049910m
7. E. Toth, L. Helm, K.E. Kellar, A.E. Merbach, Chem. Eur. J. **5**(4), 1202 (1999). doi:10.1002/(SICI)1521-3765(19990401)5:4<1202::AID-CHEM1202>3.0.CO;2-Y
8. W.J.M. Mulder, G.J. Strijkers, K.C. Briley-Saboe, J.C. Frias, J.G.S. Aguinaldo, E. Vucic, V. Amirbekian, C. Tang, P.T.K. Chin, K. Nicolay, Z.A. Fayad, Magn. Reson. Med. **58**, 1164 (2007). doi:10.1002/mrm.21315
9. J.P. Andre, E. Toth, H. Fischer, A. Seelig, H.R. Macke, A.E. Merbach, Chem. Eur. J. **5**(10), 2977 (1999). doi:10.1002/(SICI)1521-3765(19991001)5:10<2977::AID-CHEM2977>3.0.CO;2-T
10. D. Bazile, C. Prudhomme, M.T. Bassoullet, M. Marlard, G. Spenlehauer, M. Veillard, J. Pharm. Sci. **84**(4), 493 (1995). doi:10.1002/jps.2600840420
11. C.A. Nguyen, E. Allemann, G. Schwach, E. Doelker, R. Gurny, J. Pharm. Sci. **254**(1), 69 (2003). doi:10.1016/S0378-5173(02)00685-3
12. S.S. Venkatraman, P. Jie, F. Min, B.Y. Freddy, G. Leong-Huat, Int. J. Pharm. **298**(1), 219 (2005)
13. V.P. Torchilin, J. Control. Release **73**(2–3), 137 (2001). doi:S0168365901002991
14. E. Nakamuraa, K. Makinoa, T. Okanob, T. Yamamotoc, M. Yokoyama, J. Control. Release **114**(3), 325 (2006)
15. R. Gref, P. Quellec, A. Sanchez, P. Calvo, E. Dellacherie, M.J. Alonso, Eur. J. Pharm. Biopharm. **51**(2), 111 (2001). doi:10.1016/S0939-6411(00)00143-0
16. C. Perez, A. Sanchez, D. Putnam, D. Ting, R. Langer, M.J. Alonso, J. Control. Release **75**(1-2), 211 (2001). doi:10.1016/S0168-3659(01)00397-2
17. C.D. Oja, S.C. Semple, A. Chonn, P.R. Cullis, Biochim. Biophys. Acta **1281**(1), 31 (1996). doi:10.1016/0005-2736(96)00003-X
18. T. Riley, S. Stolnik, C.R. Heald, C.D. Xiong, M.C. Garnett, L. Illum, S.S. Davis, S.C. Purkiss, R.J. Barlow, P.R. Gellert, Langmuir **17**(11), 3168 (2001). doi:10.1021/la001226i
19. D.C. Litzinger, A.M.J. Buiting, N. Vanrooijen, L. Huang, Biochim. Biophys. Acta **1190**(1), 99 (1994). doi:0005-2736(94)90038-8
20. D.E. Owens, N.A. Peppas, Int. J. Pharm. **307**(1), 93 (2006). doi:10.1016/j.ijpharm.2005.10.010
21. E. Wisse, R.B. De Zanger, K. Charels, P. Van Der Smissen, R.S. McCuskey, Hepatology **5**(4), 683 (1985). doi:10.1002/hep.1840050427
22. R. Gref, G. Miralles, E. Dellacherie, Polym. Int. **48**, 251 (1999). doi:10.1002/(SICI)1097-0126(199904)48:4<251::AID-PI104>3.0.CO;2-4
23. K. Ogawara, M. Yoshida, K. Higaki, T. Kimura, K. Shiraishi, M. Nishikawa, Y. Takakura, M. Hashida, J. Control. Release **59**, 15 (1999). doi:S0168365999000152
24. J.A. Libera, H. Cheng, M.O. Cruz, M.J. Bedzyk, J. Phys. Chem. B **109**(48), 23001 (2005). doi:10.1021/jp0534941
25. F. Molnar, J. Rieger, Langmuir **21**(2), 786 (2005). doi:10.1021/la048057c
26. R. Messina, C. Holm, K. Kremer, J. Chem. Phys. **117**(6), 2947 (2002). doi:10.1063/1.1490595
27. K.F. Pirollo, J. Dagata, P. Wang, M. Freedman, A. Vladar, S. Fricke, L. Ileva, Q. Zhou, E.H. Chang, Mol. Imaging **5**(1), 41 (2006). doi:10.2310/7290.2006.00005
28. R. Gref, M. Luck, P. Quellec, M. Marchand, E. Dellacherie, S. Harnisch, T. Blunk, R.H. Muller, Colloids Surf. B Biointerfaces **18**(3–4), 301 (2000). doi:S0927-7765(99)00156-3
29. W.R. Gombotz, W. Guanghui, T.A. Horbett, A.S. Hoffman, J. Biomed. Mater. Res. A **25**(12), 1547 (1991). doi:10.1002/jbm.820251211
30. K. Bergstrom, E. Osterberg, K. Holmberg, A.S. Hoffman, T.P. Schuman, A. Kozlowski, J.H. Harris, J. Biomater. Sci. Polym. Ed. **6**(2), 123 (1994). doi:10.1163/156856294X00257
31. G. Yu, M. Yamashita, K. Aoshima, M. Takahashi, T. Oshikawa, H. Takayanagi, S. Laurent, C. Burtea, L. Vander, L. Vander Elst, R.N. Muller, Bioorg. Med. Chem. Lett. **17**(8), 2246 (2007). doi:S0960-894X(07)00117-5
32. Y. Okuhata, Adv. Drug Deliv. Rev. **37**(1-3), 121 (1999). doi:S0169-409X(98)00103-3